Realization of All-Optical Multistate Switching in an Atomic Coherent Medium

Jiteng Sheng,[1] Utsab Khadka,[1] and Min Xiao[1,2,*]

[1]Department of Physics, University of Arkansas, Fayetteville, Arkansas 72701, USA

[2]National Laboratory of Solid State Microstructures and Department of Physics, Nanjing University, Nanjing 210093, China

(Received 28 May 2012; published 30 November 2012)

We have experimentally observed optical multistability (OM) in an optical ring cavity containing three-level Λ-type Doppler-broadened rubidium atoms. The shape of the OM curve can be significantly modified by changing the power of the control laser field. An all-optical multistate switching or coding element is realized and flexibly controlled by adding a pulse sequence to the input (probe) intensity.

DOI: 10.1103/PhysRevLett.109.223906 PACS numbers: 42.65.Pc, 42.50.Gy, 32.80.Qk

Optical multistability (OM), which is known as a system to output three or more stable states for a given input state, has attracted continued interest due to its potential application in all-optical multistate switching or coding elements. Such multistate switching devices can be used for optical computing, optical communication, and quantum information processing, especially with an increased channel capacity compared to the ordinary binary optical switching based on optical bistability (OB) [1–4]. The OM phenomenon was studied in atomic vapor over 30 years ago under various conditions [5–9]. However, most of those early OM studies were based on polarization switching, which involves two coupled modes ($\sigma+$ and $\sigma-$ polarizations) typically on resonance in the same optical cavity. Recently, similar OM was also theoretically predicted [10] and experimentally realized [11] in the system with semiconductor microcavity polaritons. With the induced atomic coherence [12] in the three-level atomic system, the Kerr nonlinearity can be greatly enhanced near the electromagnetically induced transparency (EIT) resonance [13], which can significantly modify the nonlinear behaviors of the atomic medium inside an optical cavity. In 1996, Harshawardhan and Agarwal have theoretically shown that a control-field-induced OM is possible by using EIT and quantum interferences in a multilevel atomic system [14] rather than using a second cavity field. However, OM based on such mechanisms has not been experimentally demonstrated in previous studies.

In this Letter, we report the first experimental observation of this new type of OM in an optical ring cavity containing three-level Λ-type Doppler-broadened rubidium atoms in a new operating regime from the previously studied OB case [4] (i.e., at a higher temperature and with larger input, as well as control, laser powers). The physical mechanism of this type of OM is that the cavity field experiences higher-order nonlinearities (beyond the third-order Kerr effect) when it passes through the intracavity medium, which can be coherently manipulated by a control field (the coupling field for EIT). In the current system there is only one cavity field, since the control field (not on resonance in the cavity) is only used to prepare the coherent medium and generate large nonlinearity. Such an OM curve can be simply viewed as two bistable hysteresis cycles interlacing together with a controllable distance between them. This OM is quite different from the earlier experimental observation by Joshi and Xiao [15], where the observed OM is due to the coexistence of both absorptive and dispersive optical bistabilities at the same time. The great advantage of the OM observed in this work is its ability for practical applications in multistate switching or coding by adding a pulse sequence to the input (probe) intensity, as was done for the two-state OB case [16].

The basic OM phenomenon can be easily analyzed by employing the standard model of OB in a two-level system as given by Bonifacio and Lugiato [17], which was soon extended to different multilevel schemes [18–20]. Here, we consider a three-level Λ-type atomic system, as depicted in the inset of Fig. 1. The equations for the density-matrix elements under dipole and rotating-wave approximations can be derived by the standard semiclassical model as [21]

$$\begin{aligned}
\dot{\rho}_{22} &= -\Gamma_{21}\rho_{22} + \Gamma_{32}\rho_{33} + \frac{i}{2}(\rho_{32}\Omega_c^* - \rho_{23}\Omega_c),\\
\dot{\rho}_{33} &= -(\Gamma_{31}\rho_{33} + \Gamma_{32}\rho_{33}) + \frac{i}{2}(\rho_{23}\Omega_c - \rho_{32}\Omega_c^*\\
&\quad + \rho_{13}\Omega_p - \rho_{31}\Omega_p^*),\\
\dot{\rho}_{21} &= -\tilde{\gamma}_{21}\rho_{21} + \frac{i}{2}\rho_{31}\Omega_c^* - \frac{i}{2}\rho_{23}\Omega_p,\\
\dot{\rho}_{31} &= -\tilde{\gamma}_{31}\rho_{31} + \frac{i}{2}\rho_{21}\Omega_c + \frac{i}{2}(\rho_{11} - \rho_{33})\Omega_p,\\
\dot{\rho}_{32} &= -\tilde{\gamma}_{32}\rho_{32} + \frac{i}{2}(\rho_{22} - \rho_{33})\Omega_c + \frac{i}{2}\rho_{12}\Omega_p,
\end{aligned} \tag{1}$$

where $\Omega_p = \mu_{13}E_p/\hbar$ and $\Omega_c = \mu_{23}E_c/\hbar$ are the Rabi frequencies of the probe and control laser beams, respectively. We define $\tilde{\gamma}_{21} = \gamma_{21} - i(\Delta_p - \Delta_c)$, $\tilde{\gamma}_{31} = \gamma_{31} - i\Delta_p$, and $\tilde{\gamma}_{32} = \gamma_{32} - i\Delta_c$. Γ_{nm} is the natural decay rate between level $|n\rangle$ and level $|m\rangle$; and $\gamma_{nm} = \frac{1}{2}(\Gamma_n + \Gamma_m)$. Here, $\Delta_p = \omega_p - \omega_{13}$ and $\Delta_c = \omega_c - \omega_{23}$ are the frequency detunings for the probe and control beams, respectively.

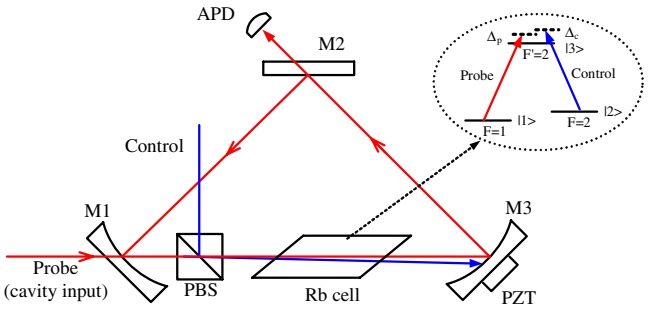

FIG. 1 (color online). Experimental setup. Polarization beam splitter (PBS); M1, M2, and M3 cavity mirrors; avalanche photodiode detector (APD); and piezoelectric transducer (PZT). Inset: the relevant atomic system.

By solving Maxwell's equations with the cavity boundary conditions under the steady-state and mean-field limits, the cavity input-output relation can be obtained as [18–20]

$$y = \frac{1 - Re^{-i\Delta_\theta}}{T} x - iC\rho_{31}. \tag{2}$$

We define the normalized input and intracavity fields as $y = \frac{\mu_{13}E_p^I}{\hbar\sqrt{T}}$ and $x = \frac{\mu_{13}E_p^O}{\hbar\sqrt{T}}$, where E_p^I (E_p^O) is the input (output) field amplitude. $C = \frac{N\omega_p l\mu_{13}^2}{2\hbar\varepsilon_0 cT}$ is the cooperativity parameter defined for OB [1,17–20]. $R(T)$ is the reflection (transmission) coefficient of the cavity mirrors (with $R + T = 1$). N is the atomic density, l is the length of the atomic sample, ε_0 is the vacuum permittivity, and c is the light speed in vacuum. The cavity frequency detuning parameter is defined as $\Delta_\theta = \omega_{\text{cav}} - \omega_{13}$.

The experimental setup is shown in Fig. 1. A three-mirror optical ring cavity is composed of an input mirror M1 and an output mirror M2 with 3% and 1.4% transmissivities, respectively; and a third mirror, M3, with reflectivity larger than 99.5% mounted on a piezoelectric transducer for cavity frequency scanning and locking. The cavity length $L = 37$ cm. The rubidium vapor cell is 5 cm long with Brewster windows, and is wrapped in μ-metal sheets for magnetic field shielding and in heat tape for temperature controlling. Three energy levels in the D1 line of ^{87}Rb atoms are used for the three-level Λ-type EIT system, as shown in the inset of Fig. 1. The control beam is injected through a polarization beam splitter which is not resonant in the cavity. The probe beam is injected into the cavity via the input mirror M1 and circulates in the cavity as the cavity field, and the output is detected by an avalanche photodiode detector. The radii of the control and probe beams are estimated to be 400 and 100 μm at the center of the atomic cell, respectively. The empty cavity finesse is about 100. When the atomic cell and PBS are included as the intracavity elements, the cavity finesse decreases down to about 48. A third laser is used to lock the cavity (not shown in Fig. 1). All three diode lasers are locked to their respective Fabry-Perot cavities. The

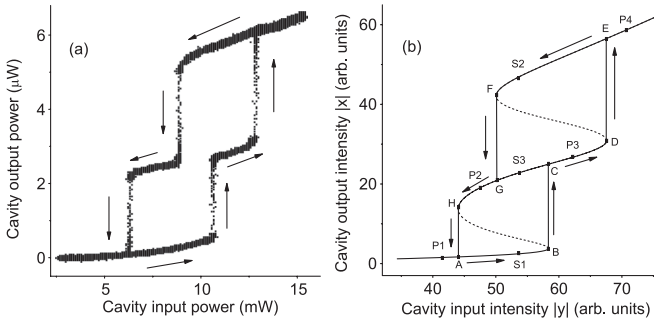

FIG. 2. (a) Experimentally observed OM curve with $P_c = 15.8$ mW, $\Delta_p/2\pi = -137.7$, $\Delta_c/2\pi = -227.7$, $\Delta_\theta/2\pi = 126.6$ MHz, and $T = 105\,^\circ$C. (b) Theoretically simulated OM curve using Eqs. (1) and (2) with appropriate parameters. Arrows indicate the directions of the cavity field evolving as the cavity input intensity scans.

triangular scan of the cavity input (probe) field is provided by an electro-optical modulator (EOM).

A typical OM curve observed in the experiment is shown in Fig. 2(a) by carefully adjusting the probe, control, and cavity detunings in certain values at a relatively high temperature ($T = 105\,^\circ$C) with the probe power (P_p) scanning triangularly from 0 to 15 mW. Other experimental parameters for Fig. 2(a) are control beam power $P_c = 15.8$ mW (the corresponding Rabi frequency is $\Omega_c/2\pi = 131.8$ MHz), $\Delta_p/2\pi = -137.7$, $\Delta_c/2\pi = -227.7$, and $\Delta_\theta/2\pi = 126.6$ MHz. Figure 2(b) is a theoretically simulated OM curve by numerically solving Eqs. (1) and (2) together. The key parameters used in the calculation are $\Omega_c/2\pi = 8$, $\Delta_p/2\pi = -4$, $\Delta_c/2\pi = -18$, $\Delta_\theta/2\pi = 5$ MHz, and $C = 500$. Here, we have only used the simple homogeneous model to obtain the typical OM curve for a qualitative comparison with the experimental curve, which indicates how the intracavity field evolves as the input power scans. In the OB case, the S-type input-output solution gives the bistable hysteresis curve with two stable states in the bistable region, since the middle part of the solution is unstable, the cavity output field jumps up or down at the so-called lower or upper turning (or threshold) point [1]. As shown in Fig. 2(b), the input-output solution shows two S-type curves and they interlace together, which gives rise to the tristability in certain input intensity region. By continuously increasing the input field power, the output intensity jumps up to a higher state first at the turning point B and then at the point D [Fig. 2(b)], when the input field power is decreased, the output intensity jumps down to a lower state first at the turning point F and then at the point H, which form a typical OM curve $ABCDEFGHA$, as shown in Fig. 2(b). In this type of OM, the output intensity can have three stable states (i.e., S1-S3-S2) at one given input intensity. Therefore, it is capable and more convenient to construct multistate switching or coding elements in such OM system, comparing to other previously demonstrated OM systems [5–9,15].

Next, by adding a pulse sequence onto the input field, we demonstrate that an all-optical multistate switch can be practically realized. We first fix the input power at ~9.5 mW under the current experimental conditions [as given in Fig. 2(a)]. Then by utilizing four different pulses [two positive and two negative pulses with different amplitudes as shown in Fig. 3(a)], a controllable triple-state switching is demonstrated as shown in Fig. 3(b). In Fig. 3(b), the initial output is at state 1 (S1), when a large positive pulse is applied, the output field first jumps from S1 to P4 [Fig. 2(b)], then it relaxes to the state S2 (upper branch) and stays there as the large pulse ends. When another small negative pulse turns on, the output field jumps down from S2 to P2 first [Fig. 2(b)], then it relaxes and stays at state S3 (middle branch). Accordingly, a large negative pulse switches the output from S3 to S1 when the pulse ends, and a small positive pulse switches the output from S1 to S3, as shown in Fig. 3. Obviously, such OM has the capability to switch the cavity output field between any two of the three states by choosing a proper pulse. In such a way, one can code a pulse sequence to perform the desired multistate switchings.

The shape of the OM curve can also be easily controlled by the control laser power, as depicted in Fig. 4. When the control beam power is low, the input-output curve is quite monochromatic and single-valued [curve (i) in Fig. 4]. When the control beam power reaches ~8 mW, the curve begins to change significantly [curve (ii)], and the bistability behavior [curve (iii)] shows up at ~10.5 mW. As the control beam power is further increased, multistability phenomenon occurs as shown in curve (iv). The typical OM shape [curve (v)] appears when the control beam power reaches to ~15.8 mW. As the control beam power increases even further, the OM curve begins to break up into two independent OB curves, and the multistability is gone, as shown in curve (vi) of Fig. 4. It is worth to point out that the cavity output curve evolves with different control beam powers as shown in Fig. 4 only under the current specially chosen experimental conditions, since different sets of detuning parameters will lead to different evolution patterns.

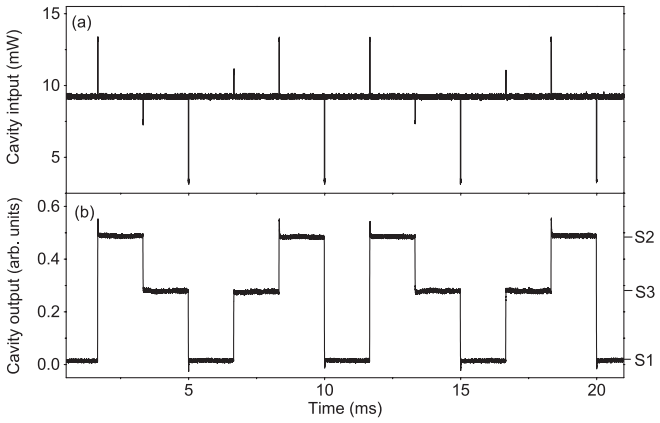

FIG. 3. Optical multistate switching. (a) Cavity input pulse sequence. (b) Controlled cavity output with three stable states.

To experimentally observe such OM phenomenon in the current system with three-level atoms in a vapor cell inside an optical ring cavity, there are certain conditions needed to be satisfied. First, a high temperature and a large input power scanning range are required. The higher cell temperature leads to a higher atomic density; therefore, higher-order nonlinearities can be made larger, for example, at $T = 105\,^{\circ}\mathrm{C}$, the atomic density can reach $\sim 8 \times 10^{12}\ \mathrm{cm}^{-3}$. A large input power scanning range is essential, since if the input power is not scanned to a large enough value, then under certain experimental conditions only part of the OM curve can be observed. For example, if the cavity input power scans from 0 to 9 mW, then either no bistability or only one bistable loop can be observed at either high or low control beam power as shown in Fig. 4 for certain special detuning values. Second, the probe and control frequency detunings should be locked around the point where the Kerr nonlinearity is large and optimal. The observed OM phenomenon is very sensitive to the frequency detuning values. It is worth to point out that the ρ_{31} term in Eq. (2) determines whether the OM is possible or not. Higher-order nonlinearities enable the multistable solutions for Eq. (2) at a fixed input intensity [see the discussion about Eq. (19) in Ref. [14]]. It was demonstrated that there are two enhanced Kerr nonlinearity peaks (one positive and one negative) around the two-photon resonant center frequency ($\Delta_p = \Delta_c$) due to atomic coherence in such three-level Λ-type system [13]. Therefore, in order to

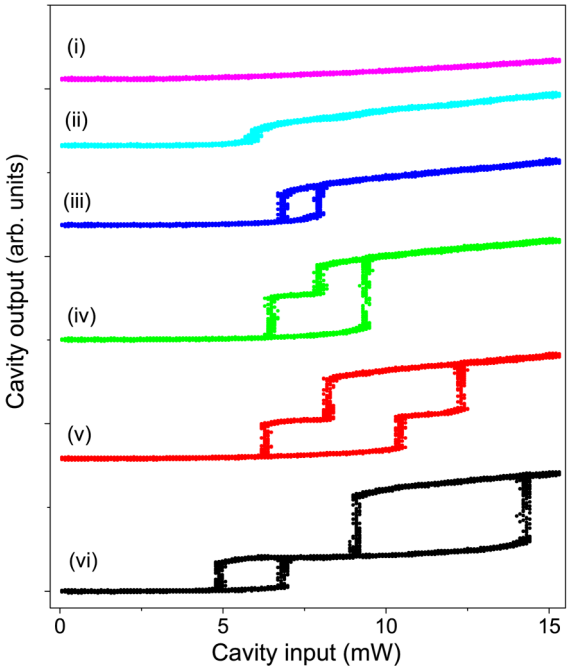

FIG. 4 (color online). Evolution of OM curves for different control beam powers at (i) 2.6, (ii) 8.0, (iii) 10.5, (iv) 13.7, (v) 15.8, and (vi) 18.9 mW. Other experimental parameters are the same as in Fig. 2.

observe OM, it is important to find large Kerr-nonlinearity points in this system by optimizing experimental parameters. In principle, the OM curve can be observed with the system at either the positive or negative nonlinear peak. Therefore, the experimental conditions make the system in Fig. 2 situate at one of the four parametric regions; i.e., (i) $\Delta_c > 0$, $\Delta_p - \Delta_c > 0$, (ii) $\Delta_c > 0$, $\Delta_p - \Delta_c < 0$, (iii) $\Delta_c < 0$, $\Delta_p - \Delta_c > 0$, and (iv) $\Delta_c < 0$, $\Delta_p - \Delta_c < 0$. However, one needs to avoid wave mixing or Raman processes at certain atomic detunings [22]. Third, after fixing one set of the chosen Δ_p and Δ_c values, we manually scan the cavity detuning Δ_θ until the OM curve occurs. The OM curve is more sensitive to the frequency detunings than to the control beam power. Especially, slight changes on the atomic detunings, i.e., Δ_p and Δ_c, will dramatically modify the OM curve and make it disappear easily. Under certain atomic detunings, four-state OM curves have also been experimentally observed, which show more complicated behaviors. Although the observed OM curves can be obtained by utilizing the simple homogeneous OB model as given in Eqs. (1) and (2). For quantitative comparisons between the experimentally observed and theoretically simulated curves, a more comprehensive model is needed to include the considerations of Doppler effect and contributions from multi-Zeeman levels in the atomic system, as well as the spatial beam profiles. Typically, the experimental parameters are much larger than the theoretical ones, such as cooperativity, atomic and cavity detunings, and Rabi frequencies, owing to the Doppler effect, as predicted for dispersive OB in two-level atoms [23].

In conclusion, we have experimentally realized a controllable multistate switching or coding element based on a new type of OM in a three-level EIT medium inside an optical ring cavity. The OM curves can be well controlled by various experimental parameters, which helps our understanding of such interesting nonlinear optical phenomenon. Such multistate system can be very useful in optical computing, optical communication, and quantum information processing [24]. Also, such OM possesses a great advancement over the traditional OB, since it is a controllable triple-well system in the potential picture; therefore, one can use it to investigate other interesting effects, such as quantum tunneling between multiple potential wells [25].

J. S. thanks Haibin Wu and Xihua Yang for their helpful discussions. M. X. acknowledges partial support from the National Basic Research Program of China (No. 2012CB921804) and NSFC (No. 11021403).

*mxiao@uark.edu

[1] L. A. Lugiato, in *Progress in Optics*, edited by E. Wolf (North-Holland, Amsterdam, 1984), Vol. XXI, p. 69.
[2] H. M. Gibbs, *Optical Bistability:Controlling Light with Light* (Academic, New York, 1985).
[3] H. M. Gibbs, S. L. McCall, and T. N. C. Venkatesan, Phys. Rev. Lett. **36**, 1135 (1976).
[4] H. Wang, D. J. Goorskey, and M. Xiao, Phys. Rev. A **65**, 011801(R) (2001); A. Joshi, A. Brown, H. Wang, and M. Xiao, *ibid.* **67**, 041801 (2003).
[5] M. Kitano, T. Yabuzaki, and T. Ogawa, Phys. Rev. Lett. **46**, 926 (1981).
[6] S. Cecchi, G. Giusfredi, E. Petriella, and P. Salieri, Phys. Rev. Lett. **49**, 1928 (1982).
[7] E. Giacobino, Opt. Commun. **56**, 249 (1985).
[8] J. Nalik, W. Lange, and F. Mitschke, Appl. Phys. B **49**, 191 (1989).
[9] G. Giusfredi, P. Salieri, S. Cecchi, and F. T. Arecchi, Opt. Commun. **54**, 39 (1985).
[10] N. A. Gippius, I. A. Shelykh, D. D. Solnyshkov, S. S. Gavrilov, Yuri G. Rubo, A. V. Kavokin, S. G. Tikhodeev, and G. Malpuech, Phys. Rev. Lett. **98**, 236401 (2007).
[11] T. K. Paraïso, M. Wouters, Y. Léger, F. Morier-Genoud, and B. Deveaud-Plédran, Nat. Mater. **9**, 655 (2010).
[12] S. E. Harris, Phys. Today **50**, No. 7, 36 (1997).
[13] H. Wang, D. J. Goorskey, and M. Xiao, Phys. Rev. Lett. **87**, 073601 (2001); Opt. Lett. **27**, 258 (2002).
[14] W. Harshwardhan and G. S. Agarwal, Phys. Rev. A **53**, 1812 (1996).
[15] A. Joshi and M. Xiao, Phys. Rev. Lett. **91**, 143904 (2003).
[16] A. Brown, A. Joshi, and M. Xiao, Appl. Phys. Lett. **83**, 1301 (2003).
[17] R. Bonifacio and L. A. Lugiato, Opt. Commun. **19**, 172 (1976); Phys. Rev. A **18**, 1129 (1978).
[18] M. A. Antón and O. G. Calderón, J. Opt. B **4**, 91 (2002).
[19] J.-H. Li, X.-Y. Lü, J.-M. Luo, and Q.-J. Huang, Phys. Rev. A **74**, 035801 (2006).
[20] M. Sahrai, S. H. Asadpour, H. Mahrami, and R. Sadighi-Bonabi, J. Lumin **131**, 1682 (2011).
[21] M. O. Scully and M. S. Zubairy, *Quantum Optics* (Cambridge University Press, Cambridge, England, 1997).
[22] J. Sheng, H. Wu, X. Yang, U. Khadka, and M. Xiao, Opt. Lett. **37**, 1655 (2012).
[23] S. S. Hassan, P. D. Drummond, and D. F. Walls, Opt. Commun. **27**, 480 (1978).
[24] R. W. Keyes, J. Phys. Condens. Matter **18**, S703 (2006).
[25] P. D. Drummond, Phys. Rev. A **33**, 4462 (1986); H. Risken, C. Savage, F. Haake, and D. F. Walls, *ibid.* **35**, 1729 (1987).